Title: Unrestrained growth of correctly oriented microtubules instructs axonal microtubule orientation

Authors: Maximilian AH Jakobs[1,*], Assaf Zemel[2], Kristian Franze[1,3,4,*]

Affiliations:

[1]Department of Physiology, Development and Neuroscience, University of Cambridge, Downing Street, Cambridge, CB2 3DY, UK.

[2]Institute of Dental Sciences and Fritz Haber Center for Molecular Dynamics, Hebrew University of Jerusalem, Jerusalem, Israel.

[3]Institute of Medical Physics, Friedrich-Alexander University Erlangen-Nuremberg, 91052 Erlangen, Germany.

[4]Max-Planck-Zentrum für Physik und Medizin, 91054 Erlangen, Germany

*Correspondence to: mj455@cam.ac.uk and kf284@cam.ac.uk

Abstract:

In many eukaryotic cells, directed molecular transport occurs along microtubules. Within neuronal axons, transport over vast distances particularly relies on uniformly oriented microtubules, whose plus-ends point towards the distal axon tip (+end out). However, axonal microtubules initially have mixed orientations, and what breaks this orientation symmetry is poorly understood. Using live imaging, physical modeling and simulations, we found that +end out microtubules surpass a growth transition and undergo persistent long-term growth. In contrast, oppositely oriented microtubules remain short. We confirmed experimentally and *in silico* that the enhanced growth of +end out microtubules is critical for achieving uniform microtubule orientation. Our data suggest that the accelerated growth kinetics of correctly oriented microtubules instructs overall axonal microtubule orientation, thus enabling efficient long-range transport essential for neuronal functioning.

One Sentence Summary: Enhanced growth of microtubules towards the axon tip is crucial for establishing microtubule order needed for molecular transport.

29 **Main Text:**

30 Symmetry breaking is critical for many biological systems. An organism starts of as a single round
31 cell that divides and differentiates into many cells, tissues and organ systems. The neuron, with
32 its branched dendrites and sometimes exceedingly long axon, is one of the least symmetric cells
33 found in animals. Axons connect neurons with distant targets and thus enable long-distance
34 signal transmission throughout the body at high speed.

35 The enormous length of axons, which can extend over several meters in some vertebrate species,
36 poses substantial logistical challenges. Proteins and genetic material originating in the cell body
37 need to be actively transported down the axon. Transport occurs along microtubules, which are
38 long, polarized polymers that undergo stochastic cycles of growth and shrinkage (**FIGURE 1A)**.
39 Motor proteins transport cargo either towards a microtubule's dynamic (i.e., growing or
40 shrinking) +end, or the stabilized -end.

41 In immature axons, microtubule orientation is mixed, with 50-80% of all microtubules having
42 their +end out. During early neuronal development, the fraction of +end out axonal microtubules
43 increases (*1*, *2*). In mature axons, ~95% of all microtubules point in the same direction (+end out)
44 (*3*, *4*), enabling polarized transport (*5*). Deficits in polarized transport have been associated with
45 human neurodegenerative diseases, such as Alzheimer's and Parkinson's disease (*5*). Despite the
46 importance of polarized transport in neuronal axons, the mechanism that breaks microtubule
47 symmetry is still poorly understood.

48 Microtubules in post-mitotic neurons are not attached to the centrosome (*6*). Nucleation of new
49 microtubules occurs from somatic Golgi (*7*) through elongation of severed pieces (*8*) or *de novo*
50 polymerization alongside existing microtubules (*9*, *10*). These newly formed microtubules often
51 orient in the same direction as existing ones, enforcing any pre-existing orientation bias (*11*, *12*),
52 which, however, by itself cannot explain the +end out orientation of microtubules in mature
53 axons. Furthermore, in axons, short microtubules pointing with their -end out can be transported
54 towards the cell body (i.e., away from the tip) by cytoplasmic dynein, a process likely assisted by
55 the microtubule bundling protein TRIM46 (*2*, *13*, *14*). However, also this mechanism is not
56 sufficient to explain how axonal microtubules orient with their +ends pointing away from the cell
57 body (see below).

58 To address how microtubule orientation in neuronal axons is achieved, we first quantified
59 microtubule growth in *Drosophila melanogaster* axons by labelling growing microtubule +ends
60 with the fusion protein EB1-GFP, which labels +ends with bright 'comets' (**FIGURE 1A-C**) (*15*). The
61 distance over which a comet moves in the axon is equal to the overall length d_g that is added to
62 a microtubule between the start of its growth cycle and the catastrophe leading to microtubule
63 shrinkage (**FIGURE 1A)**. The direction of growth highlights whether a microtubule is oriented with
64 its +end away from (+end out) or towards (-end out) the cell body. Time-lapse movies of EB1-GFP
65 comets were converted into kymographs and analyzed using *KymoButler* (*16*) (**FIGURE 1C-D**).

66 The fraction of +end out microtubules increased over time and with increasing axonal length
67 (**SUPPLEMENTAL FIGURE 1**), confirming that microtubule orientation increases during development
68 (*1*, *2*). Most microtubule growth events (~66%) were found within the first 20 µm from the

advancing axon tip (**FIGURE 1A,E**). Microtubule growth lengths per cycle, d_g , were significantly higher near the axon tip compared to further away from it (**FIGURE 1F**). Furthermore, +end out microtubules added significantly more length per growth cycle than -end out microtubules, with the highest difference between +end out and -end out microtubules (~0.5 µm/cycle) found within the first 10 µm from the axon tip (**FIGURE 1G**). Hence, the orientation of microtubules that added more length per growth cycle (i.e., +end out microtubules) became the dominant microtubule orientation during neuronal development, indicating a correlation between increased +end out microtubule growth and the fraction of +end out microtubules in axons.

On long time scales, differences in microtubule growth length per growth cycle should primarily affect average microtubule lengths l_{MT}. To test whether the rather small differences in d_g of ~0.5 µm/cycle lead to biologically meaningful differences in the average expected microtubule lengths between +end out and -end out oriented microtubules, we formulated a 2-state Master equation model of microtubule growth and shrinkage (see (*17*) & supplemental methods for details The model distinguishes two regimes (**FIGURE 2A**):

$$l_{MT} = \begin{cases} d_g d_s/(d_s - d_g) & d_s > d_g \quad \text{('bounded' growth)} \\ \infty & d_s \leq d_g \quad \text{('unbounded' growth)} \end{cases} \tag{1}$$

where d_s = lost length per shrinkage cycle.

When $d_s \leq d_g$, the average length added to the microtubule exceeds the average shrinkage length per cycle so that a microtubule will exhibit net growth and elongate as long as physically possible in its confined environment (called 'unbounded' growth). For $d_s > d_g$, however, growth is 'bounded' and average microtubule lengths follow an exponential distribution with a mean of

88 $d_s d_g/(d_s-d_g)$. In practice, this means that microtubules with $d_g \geq d_s$ would grow until encountering
89 a physical barrier (for example the axon tip), while microtubules with $d_s > d_g$ remain finite
90 (approximately 2 µm with d_s = 2.2 µm and d_g = 1 µm).

91 We determined the microtubule shrinkage per cycle d_s by co-expressing a Jupiter-mCherry fusion
92 protein (a tubulin marker) together with EB1-GFP in *D. melanogaster* axons. Microtubules
93 stopped growing when the GFP signal disappeared from their +end, indicating a catastrophe
94 event. Subsequent microtubule shrinkage was visualized by simultaneously imaging tubulin
95 (Jupiter-mCherry), and quantified by tracing the resulting tubulin edges in the dual colour
96 kymographs (**FIGURE 2B-D**). Axonal microtubule shrinkage lengths were d_s = 2.2 ± 0.2 µm / cycle
97 (mean ± s.e.m., **FIGURE 2E**). With this value for d_s, our model predicted the divergence of l_{MT} at
98 around d_g = 2.2 µm (**FIGURE 2F).** The measured values of d_g *and* d_s hence suggested that +end out-
99 oriented microtubules within 10 µm from the axon tip exhibit a considerably higher likelihood of
100 unbounded growth than -end out microtubules within that range and any microtubule further
101 away from the tip (**FIGURE 2F)**. The enhanced growth of +end out microtubules near the axon tip
102 implied a higher chance of survival for +end out microtubules while leaving -end out microtubules
103 labile, thus establishing and maintaining overall axonal +end out microtubule orientation.

104 To test this hypothesis, we decreased microtubule growth using Nocodazole, a drug that disrupts
105 microtubule polymerization. We also decreased microtubule growth by increasing the osmolarity
106 of the cell culture medium (*18*, *19*), potentially by decreasing the space for microtubules to
107 polymerize into (*20*). In both approaches, axons exhibited significantly decreased +end out
108 microtubule growth at the axon tip (< 10 µm), with d_g < 1.7µm / cycle (**FIGURE 3A-E**). In agreement

109 with our prediction, microtubules within these axons were overall significantly less uniformly
110 oriented (**FIGURE 3D-E**), confirming an important role of the enhanced growth lengths per cycle
111 of +end out microtubules in establishing axonal microtubule orientation.

112 However, why do +end out microtubules grow longer in the vicinity of the axon tip? Local
113 gradients of microtubule growth-promoting factors could lead to an increase in +end microtubule
114 growth in that region (**FIGURE 1G**). Axon tips contain a multitude of different proteins and are the
115 site of protein synthesis (*21*). Locally synthesized microtubule growth-promoting factors include
116 microtubule stabilizing proteins, such as p150 (*22*, *23*), CRMP-2 (*24*, *25*), and TRIM46 (*13*, *14*), as
117 well as free tubulin and others (*26*).

118 *Drosophila* has a p150 homologue which, similar to murine neurons(*22*), is enriched in axon (but
119 not in dendritic) tips (**FIGURE 3F, H AND SUPPLEMENTARY FIGURE 2**). These dendritic processes
120 exhibited no +end out microtubule orientation (**SUPPLEMENTARY FIGURE 3**). Inserting the measured
121 axonal p150 gradient profile into a mathematical model indicated that the observed gradient
122 should, in theory, be able to cause different growth behaviors for +end out and -end out
123 microtubules in axonal tips (**SUPPLEMENTARY FIGURE 4**). Accordingly, +end out microtubule growth
124 lengths per cycle d_g were significantly higher in axons than in dendritic processes -which exhibited
125 mixed microtubule polarities (**SUPPLEMENTARY FIGURE 3**).

126 To test this prediction further, we assessed microtubule dynamics in *wild-type*, *p150-RNAi*
127 expressing neurons, and in neurons from $p150^1$/+ mutant flies (**FIGURE 3G-K**). $p150^1$ (also known
128 as Gl^1) mutants express a truncated p150-RNA transcript, which results in a dominant negative
129 phenotype (*27*). Both the expression of *p150-RNAi* and of dominant negative $p150^1$/+ led to a

130 significant decrease in +end out microtubule growth within 10 µm from the axon tip (**FIGURE 3L**).
131 In agreement with our model, microtubule orientation was significantly decreased in both *p150-*
132 *RNAi* and *p150^{1}/+* axons compared to controls (**FIGURE 3M**), indicating that growth-promoting
133 protein gradients at the axon tip do indeed have an important role in regulating the overall
134 polarization of the axonal microtubule network.

135 Previous work showed that p150 accumulation at axon tips depends on the activity of the
136 microtubule-specific molecular motor protein kinesin 1 (*22*), which preferentially enters axons
137 over dendrites (*28*). Accordingly, disruption of kinesin 1 function with an RNAi treatment led to
138 considerable mislocation of p150 along axons (**SUPPLEMENTARY FIGURE 5A-D**). Again, the absence
139 of a p150 gradient in these neurons led to significantly decreased +end out microtubule growth
140 near the axon tip, and hence to an overall decrease in axonal microtubule orientation
141 (**SUPPLEMENTARY FIGURE 5E-I**). In addition to unbounded +end out microtubule growth identified
142 here, other mechanisms have previously been suggested to be involved in regulating the overall
143 axonal microtubule orientation, including dynein-mediated sliding of -end out microtubules
144 towards the cell body (*2*, *13*) and augmin-mediated microtubule templating, that is nucleating
145 microtubules tend to have the same orientation as existing ones in the same cellular region) (*9*,
146 *10*).

147 Computer simulations of microtubule sliding and/or templating led to a steady state in which a
148 fixed fraction of the axon length (close to the cell body), remained enriched with -end-out
149 microtubules (**FIGURE 4A,B AND SUPPLEMENTARY FIGURE 6**). Similarly, the unbounded growth of
150 +end out microtubules alone (**SUPPLEMENTARY FIGURE 6C**) also failed to capture the high fractions

151 of +end out microtubules observed experimentally at the axon entry (**FIGURE 4B**). However,
152 integrating sliding, templating, and unbounded +end out microtubule growth in the simulation
153 (assuming that the likelihood of exhibiting unbounded growth corresponds to a successful
154 nucleation event) led to axons with overall +end out microtubule orientation recapitulating our
155 experimental results (**FIGURE 4C-D AND Supplementary Figure 6**). This highlights the necessity of
156 multiple mechanisms to establish and maintain axonal microtubule orientation. Similarly, a
157 combination of different microtubule growth-promoting proteins (e.g., tubulin, TRIM46, CRMP2,
158 and/or p150) is likely to contribute to unbounded microtubule growth into the axon tip.

159 p150, which we investigated here as an example, was concentrated at axon tips but not enriched
160 at dendritic tips (**SUPPLEMENTARY FIGURE 2),** confirming that differences in the localization of
161 microtubule growth-promoting proteins correlate with differences in microtubule growth. p150
162 is mainly known for of its role in the dynactin complex, which is an important cargo adapter
163 protein for the molecular motor protein dynein (*29*). Since p150 and dynein are functionally
164 related, it is difficult to separate their individual contributions to microtubule growth and cell
165 body-directed sliding of -end out microtubules. However, it remains unclear whether p150 is
166 required for dynein-mediated microtubule sliding (*30*, *31*), and the *Drosophila melanogaster*
167 oocyte also contains a biased microtubule cytoskeleton whose orientation is, presumably,
168 maintained by p150 (*32*). Hence, while p150 is unlikely to induce unbounded microtubule growth
169 alone, it emerges as a key contributor to the establishment of microtubule orientation.

170 We propose the following model explaining the spontaneous establishment of microtubule
171 orientation in developing axons. Growth-promoting proteins accumulate at the axon tip due to

172 microtubule +end-directed transport by kinesin motors (**SUPPLEMENTARY FIGURE 5**), rendering
173 +end out microtubule growth into the axon tip unbounded. In contrast, short -end out
174 microtubules are more prone to depolymerization and/or transport away from the tip by dynein-
175 mediated cell body-directed sliding (*1*, *2*), thus contributing to the orientation bias of
176 microtubules in the axon. This bias is further enhanced by augmin-mediated templating to
177 establish and maintain a fully organized microtubule cytoskeleton (see **FIGURE 4E** for a schematic
178 summary). Future work will reveal whether other cellular systems use similar mechanisms to
179 organize their cytoskeleton.

180 **References and Notes:**

181 1. K. W. Yau *et al.*, Dendrites In Vitro and In Vivo Contain Microtubules of Opposite Polarity
182 and Axon Formation Correlates with Uniform Plus-End-Out Microtubule Orientation. *J. Neurosci.*
183 **36**, 1071–1085 (2016).

184 2. U. del Castillo, M. Winding, W. Lu, V. I. Gelfand, V. Allan, Interplay between kinesin-1 and
185 cortical dynein during axonal outgrowth and microtubule organization in Drosophila neurons.
186 *eLife Sciences*. **4**, e10140 (2015).

187 3. P. W. Baas, M. M. Black, G. A. Banker, Changes in microtubule polarity orientation during
188 the development of hippocampal neurons in culture. *J Cell Biol*. **109**, 3085–3094 (1989).

189 4. S. R. Heidemann, J. M. Landers, M. A. Hamborg, Polarity orientation of axonal
190 microtubules. *J Cell Biol*. **91**, 661–665 (1981).

191 5. S. Millecamps, J.-P. Julien, Axonal transport deficits and neurodegenerative diseases.
192 *Nature Publishing Group*. **14**, 161–176 (2013).

193 6. M. Kuijpers, C. C. Hoogenraad, Centrosomes, microtubules and neuronal development.
194 *Mol. Cell. Neurosci.* **48**, 349–358 (2011).

195 7. A. Mukherjee *et al.*, Automated kymograph analysis for profiling axonal transport of
196 secretory granules. *Medical Image Analysis*. **15**, 354–367 (2011).

197 8. W. Yu *et al.*, The Microtubule-severing Proteins Spastin and Katanin Participate
198 Differently in the Formation of Axonal Branches. *Mol. Biol. Cell*. **19**, 1485–1498 (2008).

199 9. M. M. Nguyen *et al.*, Γ-tubulin controls neuronal microtubule polarity independently of
200 Golgi outposts. *Mol. Biol. Cell*. **25**, 2039–2050 (2014).

201 10. C. Sánchez-Huertas *et al.*, Non-centrosomal nucleation mediated by augmin organizes
202 microtubules in post-mitotic neurons and controls axonal microtubule polarity. *Nat Commun*. **7**
203 (2016), doi:10.1038/ncomms12187.

204 11. F. J. Mattie *et al.*, Directed microtubule growth, +TIPs, and kinesin-2 are required for
205 uniform microtubule polarity in dendrites. *Curr. Biol.* **20**, 2169–2177 (2010).

206 12. A. Mukherjee, P. S. Brooks, F. Bernard, A. Guichet, P. T. Conduit, Microtubules originate
207 asymmetrically at the somatic golgi and are guided via Kinesin2 to maintain polarity within
208 neurons. *eLife Sciences*. **9**, 2191 (2020).

209 13. A. N. Rao *et al.*, Cytoplasmic Dynein Transports Axonal Microtubules in a Polarity-Sorting
210 Manner. *Cell Rep*. **19**, 2210–2219 (2017).

211 14. S. F. B. van Beuningen *et al.*, TRIM46 Controls Neuronal Polarity and Axon Specification
212 by Driving the Formation of Parallel Microtubule Arrays. *Neuron*. **88**, 1208–1226 (2015).

213 15. T. Stepanova *et al.*, Visualization of microtubule growth in cultured neurons via the use
214 of EB3-GFP (end-binding protein 3-green fluorescent protein). *J. Neurosci.* **23**, 2655–2664 (2003).

215 16. M. A. Jakobs, A. Dimitracopoulos, K. Franze, KymoButler, a deep learning software for
216 automated kymograph analysis. *eLife Sciences*. **8**, 168 (2019).

217 17. M. Dogterom, S. Leibler, Physical aspects of the growth and regulation of microtubule
218 structures. *Phys. Rev. Lett.* **70**, 1347–1350 (1993).

219 18. D. Bray, N. P. Money, F. M. Harold, J. R. Bamburg, Responses of growth cones to changes
220 in osmolality of the surrounding medium. *J Cell Sci*. **98 (Pt 4)**, 507–515 (1991).

221 19. A. T. Molines *et al.*, Physical properties of the cytoplasm modulate the rates of
222 microtubule growth and shrinkage. *bioRxiv*. **265**, 2020.10.27.352716 (2020).

223 20. K. Franze, Integrating Chemistry and Mechanics: The Forces Driving Axon Growth. *Annu.*
224 *Rev. Cell Dev. Biol.* **36**, 61–83 (2020).

225 21. L. A. Lowery, D. Van Vactor, The trip of the tip: understanding the growth cone machinery.
226 *Nat. Rev. Mol. Cell Biol.* **10**, 332–343 (2009).

227 22. A. J. Moughamian, E. L. F. Holzbaur, Dynactin is required for transport initiation from the
228 distal axon. *Neuron*. **74**, 331–343 (2012).

229 23. J. E. Lazarus, A. J. Moughamian, M. K. Tokito, E. L. F. Holzbaur, Dynactin subunit
230 p150(Glued) is a neuron-specific anti-catastrophe factor. *PLoS Biol.* **11**, e1001611 (2013).

231 24. N. Inagaki *et al.*, CRMP-2 induces axons in cultured hippocampal neurons. *Nat. Neurosci.*
232 **4**, 781–782 (2001).

233 25. Y. Fukata *et al.*, CRMP-2 binds to tubulin heterodimers to promote microtubule assembly.
234 *Nat Cell Biol*. **4**, 583–591 (2002).

235 26. H. Eng, K. Lund, R. B. Campenot, Synthesis of beta-tubulin, actin, and other proteins in
236 axons of sympathetic neurons in compartmented cultures. *Journal of Neuroscience*. **19**, 1–9
237 (1999).

238 27. H. H. Plough, P. T. Ives, Induction of Mutations by High Temperature in Drosophila.
239 *Genetics*. **20**, 42–69 (1935).

240 28. R. P. Tas *et al.*, Differentiation between Oppositely Oriented Microtubules Controls
241 Polarized Neuronal Transport. *Neuron*. **96**, 1264–1271.e5 (2017).

242 29. S. R. Gill *et al.*, Dynactin, a conserved, ubiquitously expressed component of an activator
243 of vesicle motility mediated by cytoplasmic dynein. *J Cell Biol*. **115**, 1639–1650 (1991).

244 30. C. M. Waterman-Storer *et al.*, The interaction between cytoplasmic dynein and dynactin
245 is required for fast axonal transport. *PNAS*. **94**, 12180–12185 (1997).

246 31. F. J. Ahmad, C. J. Echeverri, R. B. Vallee, P. W. Baas, Cytoplasmic dynein and dynactin are
247 required for the transport of microtubules into the axon. *J Cell Biol*. **140**, 391–401 (1998).

248 32. R. Nieuwburg *et al.*, Localised dynactin protects growing microtubules to deliver oskar
249 mRNA to the posterior cortex of the Drosophila oocyte. *eLife Sciences*. **6**, 711 (2017).

250 33. N. A. Bulgakova, B. Klapholz, N. H. Brown, Cell adhesion in Drosophila: versatility of
251 cadherin and integrin complexes during development. *Current Opinion in Cell Biology*. **24**, 702–
252 712 (2012).

253 34. D. T. Bergstralh, H. E. Lovegrove, D. St Johnston, Lateral adhesion drives reintegration of
254 misplaced cells into epithelial monolayers. *Nat Cell Biol*. **17**, 1497–1503 (2015).

255 35. R. P. Brendza, L. R. Serbus, J. B. Duffy, W. M. Saxton, A function for kinesin I in the posterior
256 transport of oskar mRNA and Staufen protein. *Science*. **289**, 2120–2122 (2000).

257 36. J. Schindelin *et al.*, Fiji: an open-source platform for biological-image analysis. *Nat.*
258 *Methods*. **9**, 676–682 (2012).

259 37. M. Pool, J. Thiemann, A. Bar-Or, A. E. Fournier, NeuriteTracer: a novel ImageJ plugin for
260 automated quantification of neurite outgrowth. *Journal of Neuroscience Methods*. **168**, 134–139
261 (2008).

262 38. N. A. Bulgakova, I. Grigoriev, A. S. Yap, A. Akhmanova, N. H. Brown, Dynamic microtubules
263 produce an asymmetric E-cadherin-Bazooka complex to maintain segment boundaries. *J Cell Biol*.
264 **201**, 887–901 (2013).

265 39. Y. Shimada, S. Yonemura, H. Ohkura, D. Strutt, T. Uemura, Polarized Transport of Frizzled
266 along the Planar Microtubule Arrays in Drosophila Wing Epithelium. *Dev. Cell*. **10**, 209–222 (2006).

267 40. Y. M. Yannoni, K. White, Association of the neuron-specific RNA binding domain-
268 containing protein ELAV with the coiled body in Drosophila neurons. *Chromosoma*. **105**, 332–341
269 (1997).

270 41. N. Sanchez-Soriano *et al.*, Drosophila growth cones: A genetically tractable platform for
271 the analysis of axonal growth dynamics. *Developmental Neurobiology*. **70**, 58–71 (2010).

272 42. M. C. Stone, F. Roegiers, M. M. Rolls, Microtubules have opposite orientation in axons
273 and dendrites of Drosophila neurons. *Mol. Biol. Cell*. **19**, 4122–4129 (2008).

274 43. R. J. Vasquez, B. Howell, A. M. Yvon, P. Wadsworth, L. Cassimeris, Nanomolar
275 concentrations of nocodazole alter microtubule dynamic instability in vivo and in vitro. *Mol. Biol.*
276 *Cell*. **8**, 973–985 (2017).

277 44. W. Yu, P. W. Baas, Changes in microtubule number and length during axon differentiation.
278 *Journal of Neuroscience*. **14**, 2818–2829 (1994).

279 45. M. A. H. Jakobs, K. Franze, A. Zemel, Mechanical Regulation of Neurite Polarization
280 and Growth: A Computational Study. *Biophysical Journal*. **118**, 1914–1920 (2020).

281 46. M. Jakobs, K. Franze, A. Zemel, Force Generation by Molecular-Motor-Powered
282 Microtubule Bundles; Implications for Neuronal Polarization and Growth. *Front Cell Neurosci*. **9**,
283 441 (2015).

284 47. N. Hirokawa, S. Niwa, Y. Tanaka, Molecular Motors in Neurons: Transport Mechanisms
285 and Roles in Brain Function, Development, and Disease. *Neuron*. **68**, 610–638 (2010).

286 48. D. B. Oelz, U. del Castillo, V. I. Gelfand, A. Mogilner, Microtubule Dynamics, Kinesin-1
287 Sliding, and Dynein Action Drive Growth of Cell Processes. *Biophysical Journal*. **115**, 1614–1624
288 (2018).

289

Acknowledgements:

We would like to thank Eva Pillai, Dennis Bray, Michael Takla, and Kevin Chalut for inspiring discussions and proofreading, Andreas Prokop and Cristina Melero for teaching *Drosophila* dissection techniques, and Sarah Bray, Dmitry Nashchekin, Daniel St Johnston, and Nick Brown for providing *Drosophila* strains and laboratory space to work in.

Funding: The authors acknowledge funding from the Wellcome Trust (PhD studentship 109145/Z/15/Z to MAHJ), the UK Biotechnology and Biological Sciences Research Council (Research Grant BB/N006402/1 to KF), the European Research Council (Consolidator Award 772426 to KF), and the Alexander von Humboldt Foundation (Alexander von Humboldt Professorship to KF).

Author contributions: MAHJ and KF conceived the study; MAHJ conducted all experiments, analyzed all data and developed the model, MAHJ and AZ developed the simulations, all authors discussed the study, MAHJ and KF wrote the paper with contributions from all co-authors.

Competing interests: AZ declares no competing interests, MAHJ and KF are shareholders of deepMirror (https://deepmirror.ai), a company that, amongst other things, sells custom interfaces of the freeware *KymoButler*.

Data and materials availability: All data is made available upon request.

Supplementary Materials:

Materials and Methods

Figures S1-S5

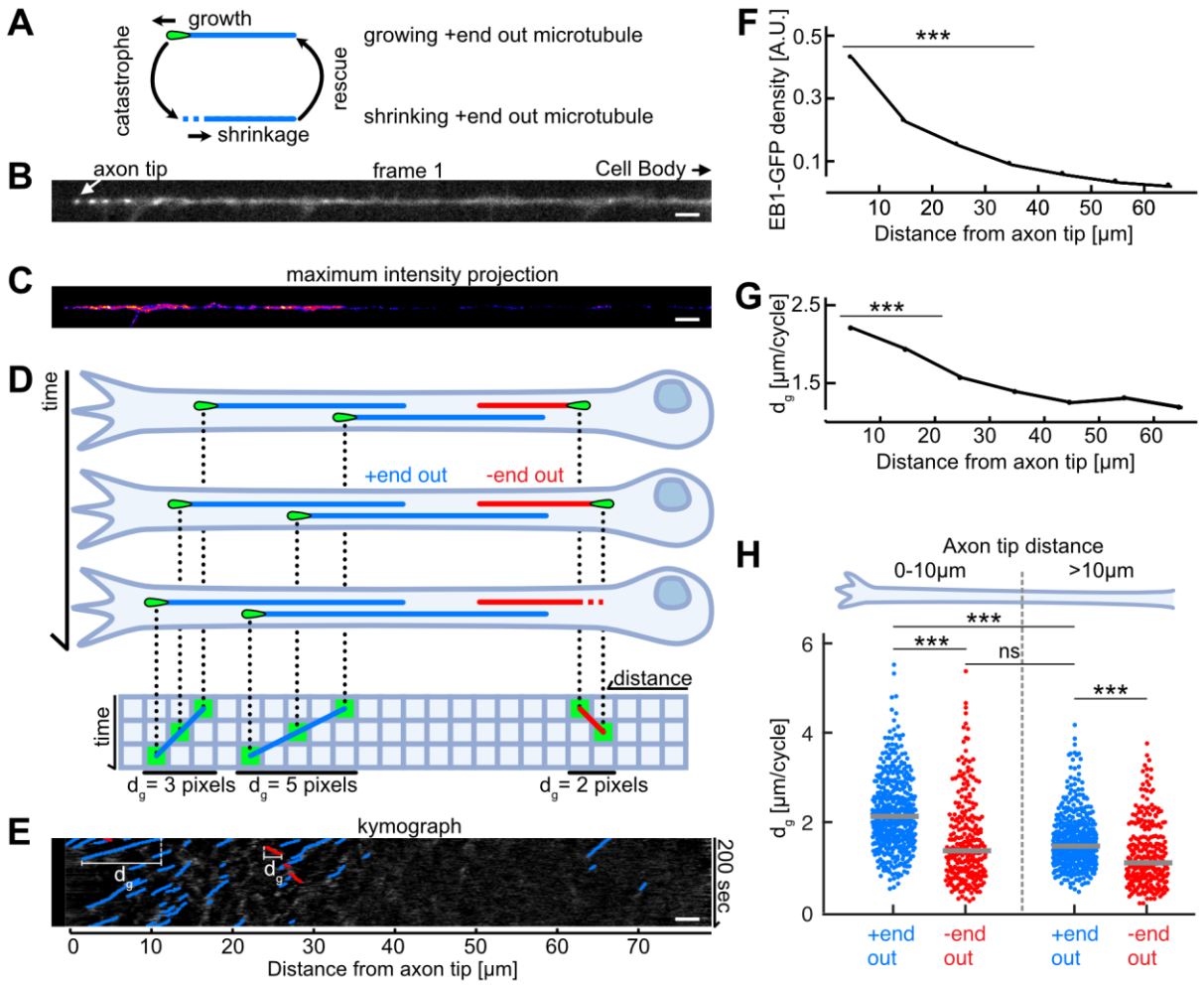

Figure 1: Axonal microtubule orientation and localization regulate microtubule growth. (A) Schematic depicting the microtubule growth and shrinkage cycle. Microtubules grow until they undergo a catastrophe, which initiates microtubule shrinkage and can start growing again after a rescue event. During growth (but not shrinkage) EB1 localizes to microtubule tips. **(B)** First frame of a live cell imaging movie of axonal EB1-GFP dynamics. Bright dots represent individual EB1-GFP puncta, which label growing microtubule +ends. **(C)** Maximum intensity projection of a 200 seconds long movie depicting EB1-GFP dynamics in a *D melanogaster* axon. EB1-GFP density is increased towards the tip. **(D)** Schematic showing how EB1-GFP live imaging movies were visualized and analyzed using kymographs. The growing tips of +end out microtubules (blue) and -end out microtubules (red) were fluorescently labelled with EB1-GFP (green tear drop shaped 'comets'). The same axon is shown at three different time points; microtubules grow at their +end, where EB1-GFP is located. The axonal intensity profiles of all time points are plotted

underneath each other, resulting in a space-time grid called 'kymograph'. Connecting puncta between consecutive kymograph lines with blue/red lines yields the overall displacement d_g for individual microtubule growth events. Note that the red -end out microtubule stops growing in the 2nd frame and shrinks in the 3rd frame **(E)** Kymograph showing EB1-GFP dynamics analyzed with *KymoButler* (*16*). Lines with a positive slope (blue, left to right upwards) are microtubules growing with their +end towards the axon tip, lines with negative slope (red, left to right downwards) are microtubules growing away from the tip. Horizontal bars indicate the growth lengths (d_g) for individual microtubule growth cycles. **(F)** EB1-GFP comet density as a function of the distance from the axon tip. Most microtubule polymerization occurred near the advancing axon tip. (N = 346, 20 biological replicates, $p < 10^{-20,}$ Kruskal Wallis test, $p < 10^{-7}$ for pairwise comparisons between bin 1-4, Dunn-Sidak post hoc test). **(G)** Microtubule added length per cycle d_g as a function of distance from the axon tip. Microtubules grew longer in the vicinity of the axon tip ($p < 10^{-20}$, Kruskal Wallis test, $p < 10^{-7}$ for pairwise comparisons of either bin 1 or 2 with any other bin, Dunn-Sidak post hoc test). **(H)** d_g for +end out (blue) and -end out (red) microtubules grouped for growth in the distalmost 10 µm of the axon tip, and further away than 10 µm from the axon tip. Each dot represents the average of one axon in the respective region, grey lines indicate median values. With d_g = 2.24 ± 0.00 µm / cycle (mean ± SEM), +end out microtubules near the axon tip grew significantly longer than -end out microtubules (d_g = 1.68 ± 0.00 µm / cycle) and microtubules located further away from the tip (N = 346 axons, 20 biological replicates; $p < 10^{-30}$, Kruskal Wallis test followed by Dunn-Sidak post hoc test; *** $p < 10^{-4}$). Scale bars: 3µm.

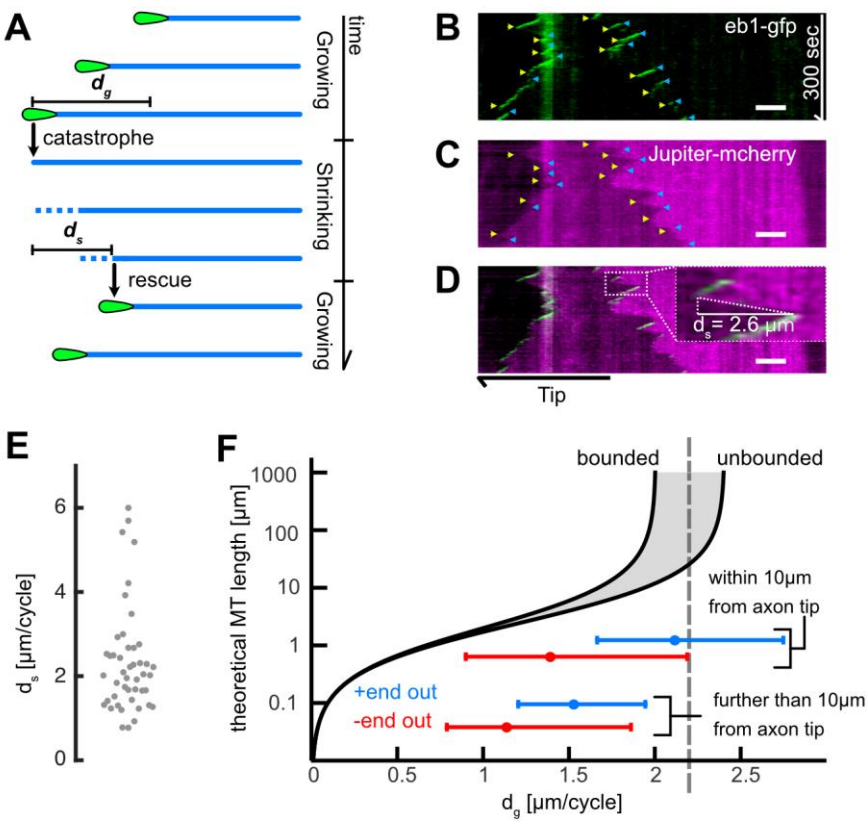

Figure 2: Microtubule length depends on growth length per cycle. (**A)** Schematic highlighting the assumptions of our two-state master equation model. Microtubules were assumed to occupy either a growing or shrinking state. During a growth cycle, the average microtubule length increases by d_g , during a shrinkage cycle, microtubule length decreases by d_s . Additionally, microtubules were able to stochastically switch between the two states as shown in **Figure 1A. (B-D)** Kymographs from a *D. melanogaster* axon that expressed **(B)** EB1-GFP (green) and **(C)** Jupiter-mCherry, a tubulin label (magenta). Individual microtubule shrinkage events, visible as **(C)** fluorescent edges and **(D)** dashed white lines in the kymograph, yielded microtubule shrinkage lengths per cycle d_s. Yellow and blue markers in **B** & **C** indicate start and end points of an individual shrinkage event and the inset in **D** highlights an individual shrinkage event. Scale bars: 3µm**. (E)** Average d_s values for N=47 axons (3 biological replicates; mean: 2.20±0.20 µm (± s.e.m). **(F)** A plot of the estimated overall microtubule length l_{MT} as a function of d_g with d_s = 2.20±0.20 µm. The two solid black lines indicate the lower and upper bounds of the average microtubule lengths for a given d_g with d_s = 2.0 or 2.4 µm. One can separate two regimes; "unbounded" and "bounded" growth, separated by a dashed line. Blue and red horizontal lines represent median ± lower and upper quantiles for +end out and -end out microtubules,

353 respectively. The top two lines represent microtubules found at the distalmost 10 µm of the axon, the bottom lines
354 microtubules found further than 10 µm away. +end out microtubules close to the tip were considerably more likely
355 to exhibit unbounded growth than +end out microtubules further away from the tip and -end out microtubules.

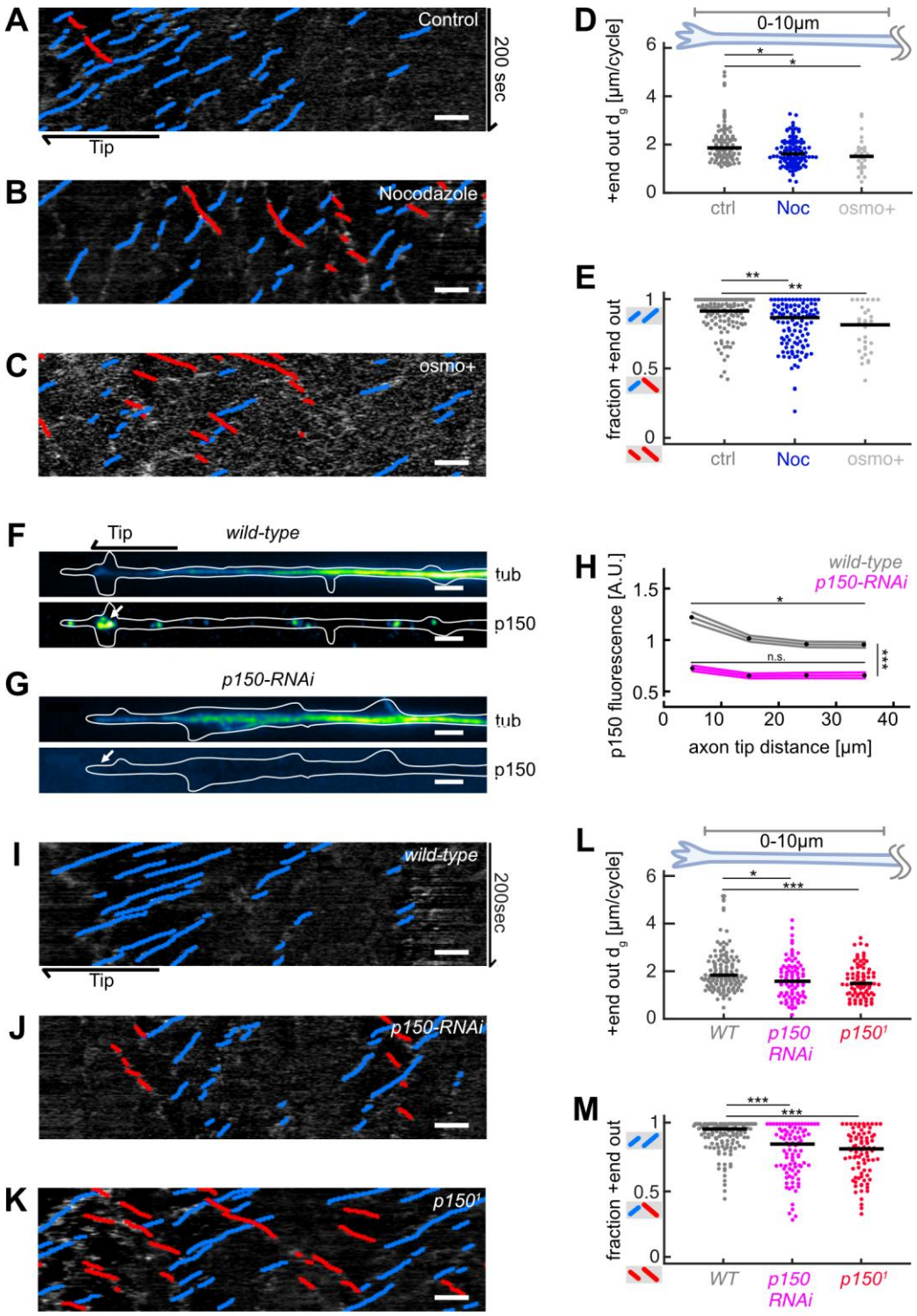

356

357 **Figure 3: Decreased microtubule growth decreases axonal microtubule orientation. (A-C)** Representative

358 kymographs analyzed with *KymoButler* (*16*) from axonal processes treated with (**A**) 0.025% DMSO (control) for 8h,

359 **(B)** 5uM Nocodazole for 8h, **(C)** medium with increased osmolarity ("osmo+") for 22h. Growth of +end out
360 microtubules is shown as blue lines, -end microtubules are red. Scale bars = 3µm. **(D)** Added growth lengths per cycle
361 d_g of +end out microtubules at the distalmost 10µm from the axon tip for control (N = 107 axons from 5 biological
362 replicates), nocodazole-treated axons (N = 116 axons from 3 biological replicates), and axons cultured in osmo+
363 medium (N = 30, 2 biological replicates). Microtubule lengths increased significantly less per growth cycle in axons
364 treated with Nocodazole or osmo+ media than controls ($p < 10^{-4}$, Kruskal Wallis test, * $p < 0.05$ for pairwise
365 comparisons, Dunn-Sidak post hoc test). **(E)** The fraction of +end out microtubules, in the different groups.
366 Microtubule orientation was calculated by counting all microtubules that grew away from the cell body (blue lines
367 in kymographs) and dividing them by all growing microtubules (blue and red). This way, a kymograph with only blue
368 lines gives a value of 1 while an equal number of blue and red lines yields a value of 0.5. Microtubules in axons
369 treated with Nocodazole or osmo+ media were significantly less uniformly oriented than those in the control group,
370 i.e., they contained a larger fraction of microtubules pointing with their +ends toward the cell body (red lines in **(A-**
371 **C)**) ($p < 10^{-4}$, Kruskal Wallis test, ** $p < 10^{-2}$ for pairwise comparisons, Dunn-Sidak post hoc test). **(F-G)** Tubulin (top)
372 and normalized p150 (bottom) immunostaining of cultured *D. melanogaster* larvae axonal processes of **(F)** controls
373 and **(G)** neurons expressing *elav-gal4* UAS driven *p150-RNAi*. Large p150 puncta were found clustered around the
374 axon tip (arrow) in controls **(F)** but not in *p150-RNAi* axons **(G)**. Scale bars = 2µm **(H)** Normalized p150 fluorescence
375 intensity as a function of distance from the axon tip for *wild-type* axons (N = 33) and *p150-RNAi* axons (N = 32, 2
376 biological replicates). Lines represent mean ± s.e.m. for *wild-type* (grey) and *p150-RNAi* (magenta). P150
377 fluorescence intensities changed along the axon ($p < 10^{-70}$; Kruskal Wallis test). In *wild-type* axons, p150 was enriched
378 at the axon tip (* $p < 0.05$ between bin 1 and bin 3 or 4; pairwise comparisons with Dunn-Sidak post hoc test), but
379 not in *p150-RNAi* expressing axons ($p > 0.05$ for all pairwise comparisons). Overall, p150 expression levels were
380 diminished in *p150-RNAi* axons compared to *wild-type* (*** $p < 10^{-7}$ for any pairwise comparison between conditions).
381 **(I-K)** *KymoButler* output for kymographs of EB1-GFP expressed in (**I**) a *wild-type* axon, **(J)** an axon expressing p150-
382 RNAi, and **(K)** an axon in a $p150^1/+$ mutant background. Scale bars = 3 µm. Blue/red lines represent microtubules
383 with +/-end out orientation, respectively. **(L)** +end out microtubule added length per cycle d_g for *wild-type* (N = 85,
384 9 biological replicates), *p150-RNAi* (N = 34, 3 biological replicates), and $p150^1/+$ (N = 83, 6 biological replicates).
385 Microtubule growth lengths were significantly decreased in both *p150-RNAi* and $p150^1$ conditions compared to

386 controls ($p < 10^{-9}$, Kruskal Wallis test, **$p < 0.001$, *$p < 0.05$, Dunn-Sidak post hoc test). **(M)** Microtubule orientation

387 for *wild-type*, *p150-RNAi*, and *p150^{1}/+*. Microtubules were less uniformly oriented in both *p150-RNAi* and *p150^{1}*

388 axons ($p < 10^{-9}$, Kruskal Wallis test, *** $p < 10^{-5}$ for pairwise comparisons with Dunn-Sidak post hoc test). Overall,

389 axonal microtubule orientation was decreased after chemical, physical, and genetic perturbations of microtubule

390 growth.

391

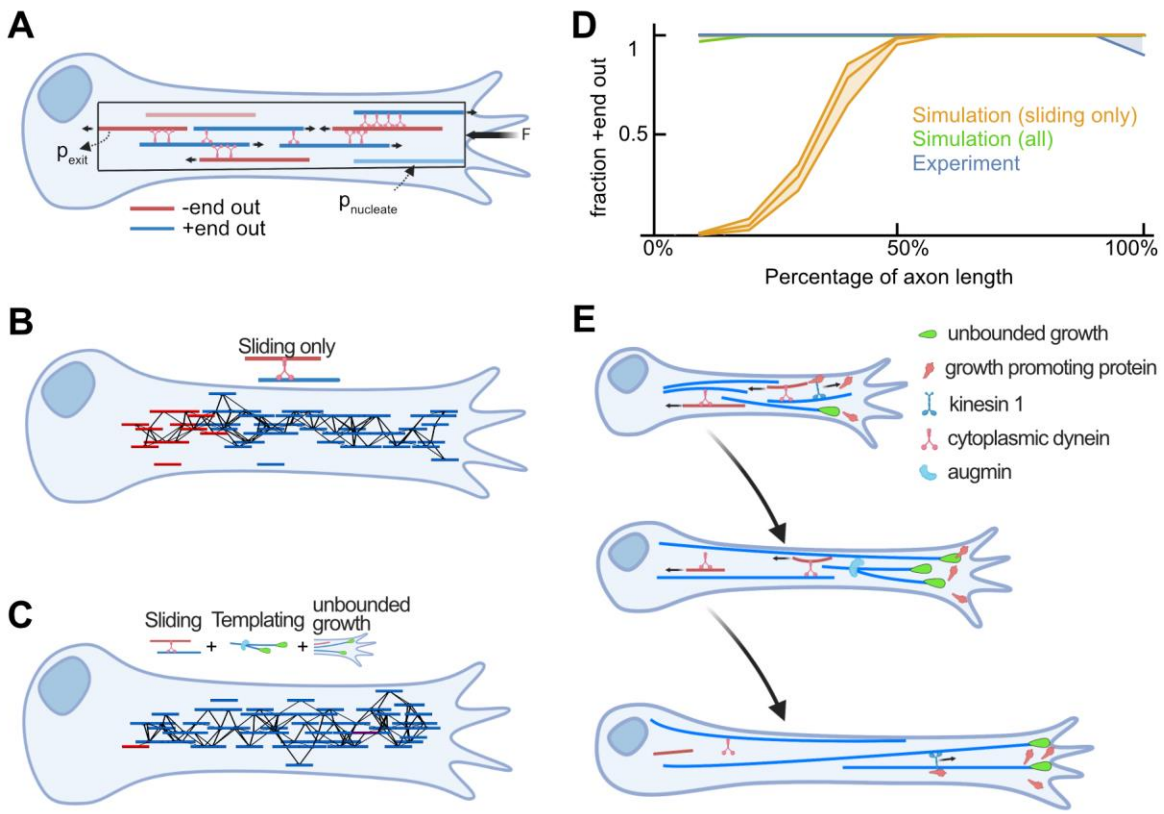

392

393 **Figure 4: Unbounded microtubule growth into the advancing axon tip is required to establish axonal microtubule**
394 **orientation. (A)** Schematic showing the microtubule sliding simulation and its relevant parameters. **(B-D)** Simulation
395 of microtubule dynamics. **(B)** Snapshot of a simulated axon with dynein-based sliding of microtubules. -end out
396 microtubules accumulated within the proximal axon. **(C)** Snapshot of an axon simulated with sliding, augmin
397 templating (new microtubules were likely oriented into the same direction as their surrounding ones), and higher
398 likelihood of unbounded growth for +end out microtubules. Much like in real axons, most microtubules were
399 oriented with their +end out throughout the axon. **(D)** Microtubule orientation along the normalized axon length for
400 the simulations with sliding only (orange trace), with sliding, templating, and unbonded growth (green), and our
401 experimental data (blue). Lines represent 30% to 70% quantiles. There was excellent agreement between the
402 experimental and *in silico data.* **(E)** Summary of proposed mechanism for establishing microtubule orientation in
403 axons. Red and blue lines represent -end out and +end out microtubules, respectively. Green drop shapes indicate
404 unbounded microtubule growth into the axon tip for +end out microtubules. Kinesin 1 deposits microtubule growth

405 promoting proteins, such as p150, at axon tips (**SUPPLEMENTARY FIGURE 4**), leading to local unbounded growth of +end

406 out microtubules. Augmin templating and cell body-directed sliding of -end out microtubules further amplifies this

407 bias. All three mechanisms together lead to a +end out microtubule cytoskeleton.